Influence of Iron Hydroxyl Phosphate Particles on the Thermal Stability and Combustible Properties of Polymethyl methacrylate

LEI WANG [a,b,c] , BAO CHENLU [a], YANG WEI [a,b,c], YUAN HU [a,c], LEI SONG [a], RICHARD K. K. YUEN [b] and ZHOU GUI [a]

a State Key Laboratory of Fire Science, University of Science and Technology of China, 96 Jinzhai Road, Hefei, Anhui 230026, P.R. China

b Department of Building and Construction, City University of Hong Kong and USTC-CityU Joint Advanced Research Centre, Suzhou, P.R. China

c Suzhou Key Laboratory of Urban Public Safety, Suzhou Institute of University of Science and Technology of China, Suzhou, P.R. China

ABSTRACT

The iron hydroxyl phosphate $Fe_{3.6}Fe_{1.02}(OH)_{2.17}(PO_4)_3O_{0.84}$(FePOH) nanoparticles were synthesized by hydrothermal method at a relative low temperature. The iron hydroxyl phosphate nanoparticles were then incorporated into poly (methyl methacrylate) (PMMA) by in situ radical polymerization. Thermogravimetric analysis (TGA) data showed that the presence of FePOH remarkably improved thermal stability and promoted the formation of char residues of PMMA matrix. For the PMMA in combination with 6 % FePOH, the heat release capacity which is an indicator of a material fire hazard was reduced by 48 %. The residue characterization and thermogravimetric analysis/fourier transform infrared spectrometry (TGA-FTIR) revealed the carbonization behavior of iron hydroxyl phosphate in PMMA matrix and probably the appearance of $Fe(CO)_5$ during the thermal decomposition of PMMA/2 %FePOH composite, which may is the reason for the improvement in the thermal and combustion properties.

KEYWORDS: poly(methyl methacrylate), iron hydroxyl phosphate nanoparticles, thermal property, combustion behavior, heat release rate, ignition, heat transfer

INTRODUCTION

Poly(methyl methacrylate) (PMMA) is an important thermoplastic material, which is mainly used as coatings and glazings [1]. However, the flammability and poor thermal stability of PMMA limit its application. It is known the methyl methacrylate (MMA) unit, which is generated during burning, brings out bubbles and further evolves into flammable gas phase. The flammable MMA gas could accelerate the weight loss rate of PMMA and leave no residue after pyrolysis even in inert atmosphere. Among the many ways of flame retardation of PMMA, the preparation of inorganic-organic hybrid composites has been considered to be one of the most effective ways, because the presence of inorganic particles can greatly improve the thermal and combustion properties of the polymeric materials [2-4]. There has been considerable interest in the fabrication of PMMA/inorganic filler composites. The inorganic materials mainly include layered double hydroxides (LDHs) [5], carbon nanotubes (CNTs) [6,7], graphite oxide [8], POSS [9,10], layered silicates [11,12] and layered phosphates [13]. In these systems, barrier formation

during combustion is the general mechanism invoked for fire retardancy. The transfer speed of heat through the char layer depends on resistance of the substrate to fire; the char formation process dominates general flame-retardant properties [5-13].

Catalyzed carbonization belongs to the condensed phase flame retardant mechanism. And general catalysts can catalyze some polymers into the char, greatly improving the thermal stability and flame retardant property of polymers. As previously reported in the literatures, phosphates (like $Zn_3(PO_4)_2$) can play a catalyzed carbonization role in many polymers [14,15]. In fact, the iron hydroxyl phosphate is also an important catalyst, which is known from a series of patents as a catalyst for the oxidative dehydrogenation of isobutyric acid to methacrylic acid. So the iron hydroxyl phosphate may have carbonization behavior, even without exotic carbon sources, in the PMMA matrix which may lead to enhanced thermal and combustion properties.

In this study, the iron hydroxyl phosphate (FePOH) nanoparticles were used as inorganic filler to enhance the thermal and combustion properties of PMMA. Firstly, the iron hydroxyl phosphate (FePOH) nanoparticles which used to be prepared by evaporating an aqueous solution of $Fe(NO_3)_3$ and $(NH_4)_2HPO_4$ or H_3PO_4 at temperatures up to 400 ˚C and performing subsequent reduction in an H_2-H_2O gas atmosphere at 450 ˚C at ambient pressures [16], were synthesized under a mild condition, using $FeCl_3$, H_3PO_4, ammonia and H_2O via the hydrothermal method at 200 ˚C. The PMMA/FePOH composites were then prepared via *in situ* radical polymerization. The structure and the dispersion of FePOH in the composites were characterized by Fourier transform infrared spectroscopy (FTIR) and scanning electron microscopy (SEM). The impact of FePOH nanoparticles on the thermal stability of the PMMA was investigated by thermogravimetric analysis (TGA). The combustion behavior of the composites was measured by the microscale combustion colorimeter (MCC). The residual char of the composites was measured by laser raman spectrometry (LRS). And the gas phase degradation products of PMMA/iron hydroxyl phosphate composites were analyzed using thermogravimetric analysis/Fourier transform infrared spectrometry (TGA-FTIR).

EXPERIMENT

Materials

Ferric chloride nine hydration ($FeCl_3 \cdot 9H_2O$), phosphoric acid (H_3PO_4), ammonia solution ($NH_3 \cdot H_2O$), benzoyl peroxide (BPO) and methyl methacrylate (MMA) were purchased from Sinopharm chemical reagent Co., LTD. All chemicals except methyl methacrylate were used as received without further purification. Methyl methacrylate was refined by vacuum distillation before used.

Synthesis

Preparation of iron hydroxyl phosphate nanoparticles

The hydrothermal synthesis was carried out in polytetrafluoroethylene-lined stainless steel containers under autogeneous pressures. The reaction of $FeCl_3$, H_3PO_4, ammonia and H_2O in the mole ratio of 1:3.6:4.2:444 at 160 ˚C for 64 h produced $Fe_{3.6}Fe_{1.02}(OH)_{2.17}(PO_4)_3O_{0.84}$ (FePOH), as kelly nanoparticles. The optimal

conditions required addition of $FeCl_3$ (3.32 mmol) to the 50ml PTFE-lined acid digestion bomb followed by H_2O (16 ml). Then ammonia (0.56 ml) and H_3PO_4 (0.42 ml) were added with stirring. Upon completion of the reaction and cooling to room temperature, kelly nanoparticles of FePOH were collected, washed with water, and dried in the air.

Preparation of PMMA/FePOH composites

PMMA/FePOH composites with different concentrations of FePOH were prepared by *in situ radical* polymerization. The appropriate amounts of freshly prepared FePOH dispersed in a certain amount of ethanol by ultrasonic were mixed with 15 g MMA monomer under stirring. When the additives were completely dispersed, 0.1 wt% of benzoyl peroxide (BPO) was added. After that, the suspension was stirred using a magnetic stirrer at 60 ˚C for 30 minutes. Then the mixture was heated and stirred at 80 °C until it formed a viscous paste (about 2 hour). Finally, the viscous paste was transferred into a mold to complete the polymerization and remove the residual solvent and unconverted MMA monomer at 80 °C for 48 hours. The corresponding PMMA/FePOH composite samples with different concentrations of FePOH were listed in Table. 1.

Characterization

X-ray Diffraction (XRD) Analysis

X-ray diffraction (XRD) patterns were performed on the 1mm thick films with a Japan Rigaku D/Max-Ra rotating anode X-ray diffractometer equipped with a Cu–Ka tube and Ni filter (*l*¼0.1542 nm).

Transmission Electron Microscopy (TEM)

Transmission electron microscopy (TEM) images were obtained on a Jeol JEM-100SX transmission electron microscope with an acceleration voltage of 100 kV. Specimens for the TEM measurements were obtained by placing a drop of sample suspension prepared by ultrasonic dispersion on a carbon-coated copper grid, and dried at room temperature.

Fourier transform infrared spectroscopy (FTIR)

Fourier transform infrared spectroscopy (FTIR) (Nicolet 6700 FT-IR spectrophotometer, Thermo Fisher Scientific, USA) was employed to characterize the DPHA using thin KBr disc. The transmission mode was used and the wavenumber range was set from 4000 to 500 cm^{-1}.

Scanning Electron Microscopy (SEM)

The morphologic structures were observed by scanning electron microscopy (SEM) Hitachi X650.

Thermogravimetric Analysis (TGA)

Thermogravimetric analysis (TGA) was carried out using a TGA Q500 thermo-analyzer instrument (TA CO., USA) from 30 to 500 ˚C at a linear heating rate of 20 ˚C/min under an air/nitrogen flow of 60 ml/min. Samples were measured in an alumina crucible with a mass of about 10 mg. The temperature reproducibility of the instrument is ±1 ^{o}C, while the mass reproducibility is ±0.2 %.

Thermogravimetric Analysis-Fourier Transforms Infrared Spectrometry (TGA-FTIR)

TGA-FTIR of the samples was performed using the TGA Q5000 IR thermo-gravimetric analyzer that was interfaced to the Nicolet 6700 FT-IR spectrophotometer. About 5.0 mg of the samples were put in an alumina crucible and heated from 30 to 500 ˚C. The heating rate was 20 ˚C/min (nitrogen atmosphere, flow rate of 45 ml/min).

Laser Raman Spectrometry (LRS)

Laser raman spectroscopy (LRS) measurements were carried out at room temperature with a SPEX-1403 laser raman spectrometer (SPEX Co., USA) with excitation provided in back-scattering geometry by a 514.5 nm argon laser line.

Microscale Combustion Calorimeter (MCC)

A GOVMARK MCC-2 Microscale combustion calorimeter (MCC) was used to record the heat release rate (HRR). In this system, about 5 mg samples were heated to 700 ˚C at a heating rate of 1 ˚C /s in a stream of nitrogen flowing at 80 cm^3/min. The volatile, anaerobic thermal degradation products in the nitrogen gas stream were mixed with a 20 cm^3/min stream of pure oxygen prior to entering a 900 ˚C combustion furnace. Measured during the test was the heat release rate d Q/d t (W) and sample temperature as a function of time at constant heating rate. The specific heat release rate HRR (W/g) was obtained by dividing d Q/d t at each point in time by the initial sample mass. The heat release capacity (HRC) was a molecular level flammability parameter that was a good predictor of flame resistance and fire behavior when only research quantities were available for testing.

RESULTS AND DISCUSSION

Characterization of FePOH

The structure of FePOH was characterized by TEM and XRD. The TEM image is shown in Fig. 1. It is observed that the average size of the FePOH nanoparticles is about 50 nm. This structure type can be regarded as the built up of infinite chains of face-sharing oxygen octahedra which are interconnected via PO_4 tetrahedra and common oxygen or hydroxyl ions. The face-sharing octahedra are fully occupied whereas in $Fe^{3+}{}_4(OH)_3(PO_4)_3$, pairs of Fe^{3+} ions are present which are separated by an empty octahedron [17]. The XRD pattern (Fig. 2) of FePOH is in agreement with the literature (space group *I*41/*amd*, a:5.2427, c:12.852, V:353.24) [17]. Figure 3 shows the TGA curve of FePOH. It can be seen that the weight loss is attributed to water departures, corresponding to 1.15 mol water per mol solid. This value is close to the theoretical value(1.09 mol water per mol solid), which is calculated through the dehydroxylation of per mol hydroxyl iron phosphate particles. Excess water, which got under the lower temperatures, may be attributed to the emission of H_2O from the surface of hydroxyl iron phosphate particles.

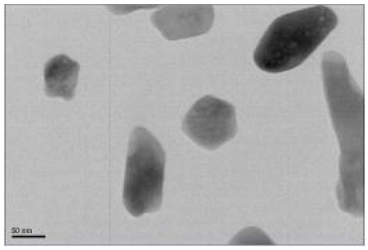

Fig. 1. A typical TEM image of the FePOH nanoparticles.

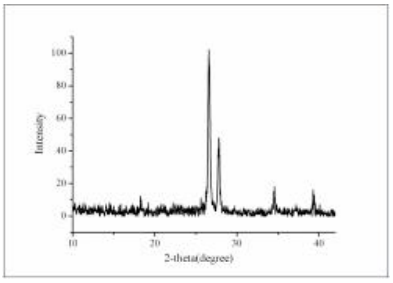

Fig. 2. The XRD pattern of the FePOH nanoparticles.

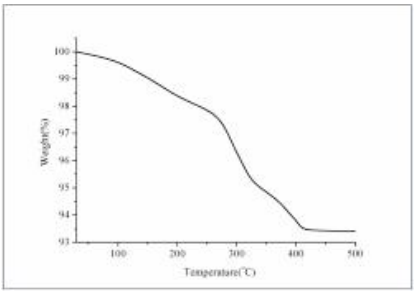

Fig. 3. TG curve of the FePOH nanoparticles.

Fourier Transform Infrared Spectroscopy (FTIR) and Dispersion of PMMA/FePOH Composite

The FTIR spectrum of the composite is shown in Fig. 4. In the spectrum, a broad band in the region at about 3440 cm^{-1} may be due to the presence of external water molecules. The peaks at 569, 603, 1080 and 1033 cm^{-1} are assigned to P–O bond which shows the existence of PO_4^{3-} group. In the PMMA/FePOH composite, the characteristic peak of PO_4^{3-} group at 1070 cm^{-1} in FePOH has red shifted to 1080 cm^{-1}, which suggests the possible linkage between FePOH and the PMMA matrix. The characteristic stretching vibration peak of carbonyl bond of PMMA at 1660 cm^{-1} also can be observed clearly in PMMA/FePOH composite. Two stretching vibration peaks appear at 2997 and 2950 cm^{-1} corresponding to CH_2 and CH_3. The peak at 1450 cm^{-1} is attributed to the vibration mode of alkane in PMMA, and peaks at 1242 and 1148 cm^{-1} are the stretching vibration of C–O bond. From the analysis of FTIR spectra, the characteristic peaks of both the FePOH and PMMA matrix are identified in the spectra of the composite. The peak at 461, 770 cm^{-1} are due to the presence of metal-oxygen stretching vibrations [18, 19]. These characteristic stretching

frequencies are also in close resemblance with the inorganic FePOH and hybrid PMMA/FePOH, indicating the binding of inorganic precipitate with organic polymer and formation of 'organic–inorganic' hybrid 'PMMA/FePOH'.

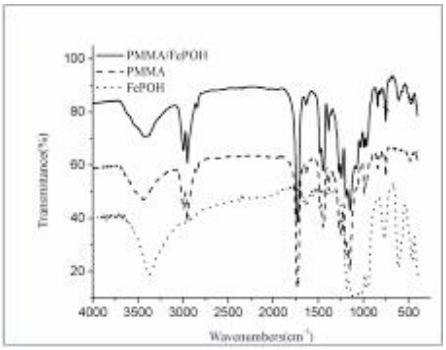

Fig. 4. The fourier transform infrared spectroscopy of PMMA, FePOH and PMMA/FePOH composite.

The SEM images of cryogenically broken surfaces can reflect the inner structure of PMMA/FePOH composite. It can be observed from Fig. 5a and Fig. 5b **(**the black line inside in Fig 5a**)** that after polymerization, FePOH particles exhibit the small range of the reunion, then uniformly disperse in the PMMA/FePOH composite (2.0 wt%). The electronic struck is the reason for the bulging place, shown in the form of white stripes in Fig. 5.

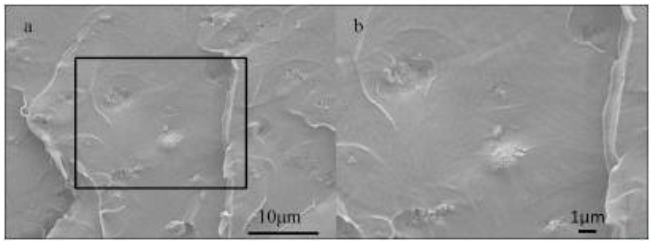

Fig. 5. SEM image of PMMA/2%FePOH composite.

Thermal Stability of PMMA/FePOH Composite

TGA is one of the most widely used techniques for rapid evaluation of the thermal stability for various polymers [20]. Figure 6 shows the TGA and DTG curves of pure PMMA and PMMA/FePOH composites with different loadings of FePOH in air atmosphere. 10 % ($T_{-0.1}$) and 50 % ($T_{-0.5}$) weight loss temperatures are listed in Table 1. Figure 6(a) shows that FePOH pushes the TGA curves of the composites towards the corresponding pristine PMMA in air atmosphere. From Table 1, it is summarized that the $T_{-0.1}$ of almost all the composites are higher than pure PMMA, except for PMMA/0.6 %FePOH sample, which may be attributed to the more removal of volatile low molar mass components. With the increasing concentration of FePOH, $T_{-0.1}$ of the samples is promoted, which indicates that the presence of FePOH defers the initial thermal degradation of PMMA. It is noticed that with 2 wt% FePOH, the $T_{-0.1}$ only promote 1 °C, but when the concentration of FePOH reaches 6 wt%, $T_{-0.1}$ of the composite is 19 °C higher than pure PMMA. For $T_{-0.5}$ of the samples, after adding FePOH, $T_{-0.5}$ of the composites with different concentration are enhanced.

When the adding amounts of FePOH are 2 and 6 wt%, $T_{-0.5}$ of the samples are increased to 323 and 342 °C, which are 15 and 34 °C higher than pure PMMA. $T_{-0.5}$ of these two samples shows significant enhancement by comparing with pure PMMA. The changing tendency of $T_{-0.5}$ is similar with $T_{-0.1}$. Meanwhile, the more amount of FePOH added, the more amount of the residue quantity remained. These results suggest that incorporating FePOH into PMMA will retard the thermal degradation of PMMA and remarkably encourage the formation of char residues of PMMA matrix.

Table. 1. TGA data of PMMA/FePOH composites with various concentrations of FePOH in air atmosphere and nitrogen atmosphere.

Sample	**Concentration of FePOH (wt%)**	**TGA data**					
		under air atmosphere			**under nitrogen atmosphere**		
		$T_{-0.1}$ (°C)	**$T_{-0.5}$ (°C)**	**Residue (%) at 600˚C**	**$T_{-0.1}$ (°C)**	**$T_{-0.5}$ (°C)**	**Residue (%) at 600˚C**
PMMA	0	231±1	308±1	0.9 ±0.2%	260±1	355±1	0 ±0.2%
PMMA/0.6%FePOH	0.6	219±1	308±1	1.8 ±0.2%	209±1	342±1	1.6 ±0.2%
PMMA/2%FePOH	2	232±1	323±1	4.5 ±0.2%	221±1	362±1	3.2 ±0.2%
PMMA/6%FePOH	6	250±1	342±1	12.2 ±0.2%	249±1	363±1	8 ±0.2%

Figure 6(b) shows the DTG curves of pure PMMA and PMMA/FePOH composites. The DTG curve of pure PMMA is characterized by three peaks (180, 240 and 310 °C). The first peak corresponds to the removal of volatile low molar mass components. The second peak indicates the depolymerization initiated by the saturated chain ends, whereas the third peak represents the depolymerization started by the random main chain scission. And the DTG curves of PMMA/FePOH composites contain one peak at about 200 °C. This mass loss (about 3~6 %) should be also attributed to the removal of volatile low molar mass components. The other two peaks almost shift to the higher temperature region than that of pure PMMA, implying the improvement of thermal stability.

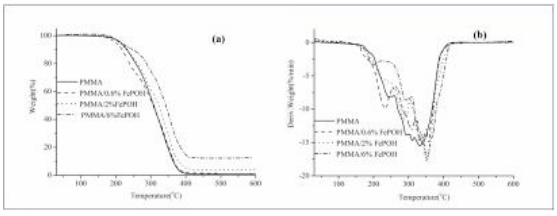

Fig. 6. (a) TGA and (b) DTG curves of pure PMMA and PMMA/FePOH composites under air atmosphere at heating rate of 20 ˚C/min.

TGA and DTG curves of the PMMA/FePOH composite under nitrogen atmosphere are shown in Fig. 7. The thermal degradation under nitrogen of the free radically prepared PMMA proceeds in three steps corresponding to the head-to-head linkage (ca. 165 °C), the chain-end initiation from the vinylidene ends (ca. 270 °C), and the third step, referred to as random scission within the polymer chain (ca. 360 °C) [21]. From the Fig. 7, the accession to FePOH does not obviously improve the thermal stability of PMMA matrix under nitrogen atmosphere. But the amount of the residue quantity is greatly enhanced, when FePOH added. And the trend is similar with that under air condition. These results demonstrate that the presence of FePOH can reduce the decomposition of PMMA and inhibit the release of volatiles.

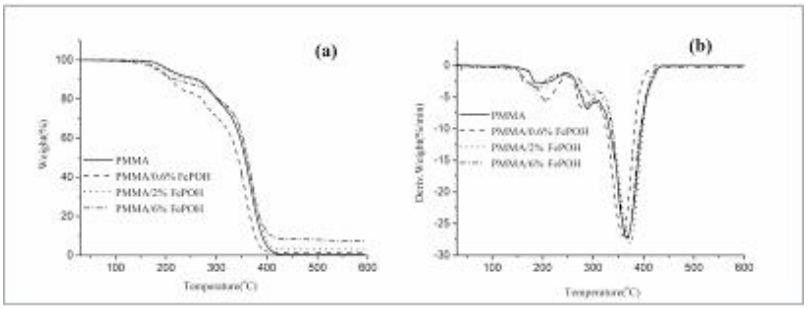

Fig. 7. (a)TGA and (b)DTG curves of pure PMMA and PMMA/FePOH composites under nitrogen atmosphere at heating rate of 20 ˚C/min.

The Thermal Combustion Properties about PMMA/FePOH Composite

The thermal combustion properties of pure PMMA and PMMA/FePOH composites were studied by means of microscale combustion calorimeter (MCC), which can provide various combustion data, including heat release rate (HRR), heat release capacity (HRC), total heat release (THR) and temperature at peak heat release rate (T_{PHRR}). A reduction of PHRR for PMMA/FePOH is observed in the heat release rate curve (Fig. 8). When FePOH is added to PMMA, PHRR value decreases from 232 W/g for PMMA to 167 W/g for PMMA/2 %FePOH with a reduction of 28 %, and to 122 W/g for PMMA/6 %FePOH with a reduction of 47 %, respectively. The data show that the PHRR decreases evidently. The reason is probably attributed to the presence of FePOH can promote the formation of a protective char and the char layers can protect the underlying materials from further burning.

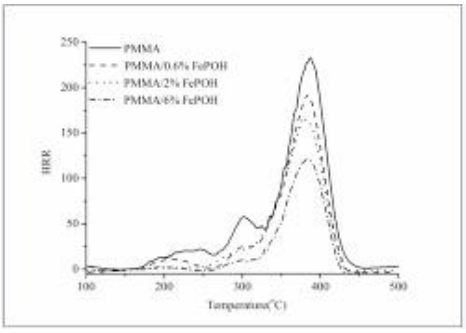

Fig. 8. HRR curves of the PMMA/FePOH composites from microscale combustion calorimeter testing.

The heat release capacity (HRC) and total heat release (THR) are also important measures of the fire hazard of a material. From HRC and THR values for all composites (Table 2), it is clearly seen that the largest reduction is still attributed to the composites in combination with FePOH. Compared with PMMA, the HRC and THR value of PMMA/2 %FePOH are reduced by 29 % and 25 %, and those values for PMMA/6 %FePOH decrease by 48 % and 47 % respectively. At the same time, the T_{PHRR} value also increases slightly. Based on the thermogravimetric analysis, it has been known that FePOH could enhance the carbonization of PMMA in the thermal decomposition process. The condensed-phase products resulting from the carbonization reaction may cover the residues to obstruct or cut off the mass transfer path to reduce the concentration of combustible gases. Thus, the THR values detected are low. Therefore, the fire hazards of the materials are reduced by the introduction of FePOH.

Table. 2. MCC data of PMMA/FePOH composites with various concentrations of FePOH.

Sample	Concentration of FePOH (wt%)	Calculated MCC data			
		HRC (J/g·k)	THR (KJ/g)	PHRR (W/g)	T_{PHRR} (°C)
PMMA	0	235± **5**	16.3± 0.1	232± **5**	379.6± 2
PMMA/0.6%FePOH	0.6	192± **5**	15.4± 0.1	191± **5**	379.7± 2
PMMA/2%FePOH	2	168± **5**	12.3± 0.1	167± **5**	381.3± 2
PMMA/6%FePOH	6	123± **5**	8.7± 0.1	122± **5**	383.2± 2

Structure Analysis of the Purified Char Residue

In order to further understand the improved flame retardancy, the chars of the sample calcined at 600 °C for 10 min in muffle furnace were investigated by Laser raman spectroscopy (LRS). Figure 9 shows the raman pattern of the char without acid treatment. It contains three obvious vibrating peaks. The peak at 1590 cm^{-1} (G-band) corresponds to the graphite hexagonal E_{2g} pattern. The vibration on the condition of sp^2 heterozygous indicates the existence of carbon graphite [24]. The peak at 1360 cm^{-1} (D-band) is attributed to amorphous carbon or the vibration of bo state swing carbon atom [22,23]. The band around 1089 cm^{-1} is assigned to the vibration mode of PO_4^{3-}.

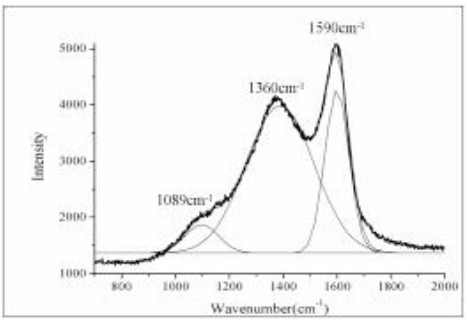

Fig. 9. Raman spectra of the purified char residue of PMMA/2%FePOH composite.

The graphitized char formatted during thermal degradation or combustion is very important in the inhibition of heat transfer because they are very stable at high temperature. The results of LRS confirm the graphitization of the residual char resulting in the improvement of the combustion properties of the composite.

The Pyrolysis Products about PMMA/FePOH Composite

The thermogravimetric analysis-Fourier transform infrared spectroscopy (TGA-FTIR) was used to analyze the thermal decomposition process. Figure 10 and Fig. 11 respectively show the intensity of the total released gas and the alkane, carbonyl groups during thermal degradation of PMMA and its composite. It is found that the evolved products are reduced when adding 2 wt% FePOH to PMMA, indicating the retardation of the thermal decomposition of the composite. It may also be attributed to the carbonization effect of FePOH during the decomposition of PMMA/FePOH composite. What is more, from Fig. 12, the groups at 2013 cm^{-1} during thermal degradation of pure PMMA and PMMA/2 %FePOH composite appear, and the amount of the groups at 2013 cm^{-1} from PMMA/2 %FePOH composite is more than that from EVA. 2013 cm^{-1} from pure PMMA attributed to C≡C, –C=C=O and so on. But apart from these groups, 2013 cm^{-1} from PMMA/2 %FePOH may also refers to $Fe(CO)_5$, which means that there probably exists vapor retardant mechanism [25]. And the time of the decomposition is advanced slightly, which may caused by the more removal of volatile low molar mass components at lower temperatures, consistent with TGA data under nitrogen atmosphere.

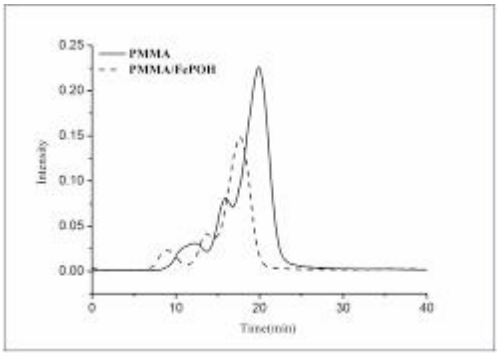

Fig. 10. The intensity of the total released gas of during thermal degradation of pure PMMA and PMMA/2 % FePOH composite under nitrogen atmosphere at heating rate of 10 ˚C/min.

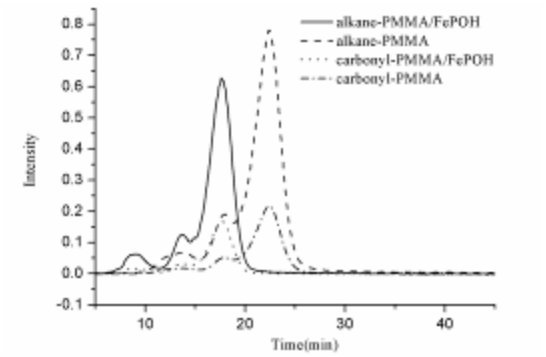

Fig. 11. The intensity of the alkane, carbonyl groups during thermal degradation of pure PMMA and PMMA/2 %FePOH composite under nitrogen atmosphere at heating rate of 10 ˚C/min.

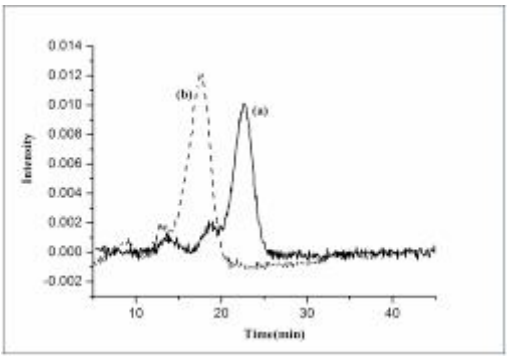

Fig. 12. The intensity of the groups at 2013 cm^{-1} during thermal degradation of (a) pure PMMA and (b) PMMA/2 %FePOH composite under nitrogen atmosphere at heating rate of 10 ˚C/min.

In combination with the results of LRS, it is indicated that the addition of FePOH slows down the decomposition of PMMA and inhibits the release of flammable gases due to the formation of graphitized char during thermal degradation or combustion of PMMA/FePOH composites. The formation of graphitized char demonstrates the termination of chain degradation. On one hand, the decomposition is restrained by the termination leading to the reduction of combustible gases. On the other hand, the graphitized char has a effective protection preventing the thermal feedback from a fire to the substrate. Furthermore, $Fe(CO)_5$ may appears during the thermal decomposition of PMMA/2 %FePOH composite, which suggests that there may also exists gas system retardant mechanism [25].

CONCLUSION

In this study, the FePOH nanoparticles were synthesized by hydrothermal method at a relative mild condition. FePOH was then incorporated into poly(methyl methacrylate) (PMMA) by *in situ* radical polymerization. The TGA results showed that the thermal stability and char yields of the composites were significantly enhanced in comparison with pure PMMA. In the MCC testing, the PHRR value decreases from 232 W/g for PMMA to 167 W/g for PMMA/2 %FePOH with a reduction of 28 %, and to 122 W/g for PMMA/6 %FePOH with a reduction of 47 %. The HRC and THR value of PMMA/2 %FePOH are reduced

by 29 % and 25 %, and those values for PMMA/6 %FePOH decrease by 48 % and 47 % respectively, which mean that the fire hazards are reduced by the introduction of FePOH. Raman spectra proved the graphitization of carbon residue. During the analysis of TGA-FTIR, it was found that the total released gas, the alkane and carbonyl groups of PMMA/FePOH composite were all lower than those of pure PMMA. The results demonstrated the carbonization behavior of iron hydroxyl phosphate in PMMA matrix and probably the appearance of $Fe(CO)_5$ during the thermal decomposition of PMMA/2 %FePOH composite, which leads to the improvement in the thermal and combustion properties. And the possibility of using polymer itself as the carbon source during thermal degradation by adding appropriate charring reagent, even the polymer like PMMA generated no carbonaceous char during combustion.

REFERENCES

[1] Domininghaus,H., *Plastics for Engineers: Materials, Properties, Applications,* Hanser Gardner Publications, New York, 1993,p.181–200.

[2] Taylor, H. S. and Tobolsky, A.V.,(1945) Radical Chain Processes in Vinyl and Diene Reactions, Journal of the American Chemical Society 67(12): 2063-2067,http://pubs.acs.org/doi/abs/10.1021/ja01228a003

[3] Alexandre, M., Beyer, G., Henrist, C., Cloots, R., Rulmont, A., Jerome, R. and Dubois, P.,(2001) "One-pot" Preparation of Polymer/Clay Nanocomposites Starting from Na+ Montmorillonite Melt Intercalation of Ethylene-vinyl Acetate Copolymer, Chemistry of Materials 13(11): 3830-3832,http://pubs.acs.org/doi/abs/10.1021/cm011095m

[4] Pack, S., Kashiwagi, T., Stemp, D., Koo, J., Si, M., Sokolov, J.C. and Rafailovich, M.H.,(2009) Segregation of Carbon Nanotubes/Organoclays Rendering Polymer Blends Self-Extinguishing, Macromolecules 42(17):6698-6709. http://pubs.acs.org/doi/abs/10.1021/ma900966k

[5] Wang, L.J., Su, S.P.,Chen, D. and Wilkie, C.A.,(2009) Fire Retardancy of Bis[2-(methacryloyloxy)ethyl] Phosphate Modified Poly(methyl methacrylate) Nanocomposites containing Layered Double Hydroxide and Montmorillonite, Polymer Degradation and Stability 94(7):1110-1118, http://www.sciencedirect.com/science/article/pii/S0141391009001098

[6] Takashi, K.; Fangming, D.; Karen, I. W.; Katrina, M. G.; John, R. S.; Severine, P. B.; Hansoo, K.; Jack, F. D., (2005) Flammability properties of polymer nanocomposites with single-walled carbon nanotubes: effects of nanotube dispersion and concentration, Polymer 46(2):471–481, http://www.sciencedirect.com/science/article/pii/S0032386104010791

[7] Takashi, K.; Jeffrey, F.; Jack, F. D.; Kazuya, Y.; Alan, N. H.; Stefan, D. L.; Jan, O.; Fangming, D.; Sheng, L.G.; Minfang, M.; Karen, I. W.; Reto, H., (2007) Relationship between dispersion metric and properties of PMMA/SWNT nanocomposites, Polymer 48(16): 4855-4866, http://www.sciencedirect.com/science/article/pii/S0032386107005812

[8] Jiang, S.h.; Gui, Z.; Bao C.L.; Dai, K.; Wang, X.; Zhou, K.Q.; Shi, Y.Q.; Lo, S. M.; Hu, Y., (2013) Preparation of functionalized graphene by simultaneous reduction and surface modification and its polymethyl methacrylate composites through latex technology and melt blending, Chemical Engineering Journal 226(15):326–335, http://www.sciencedirect.com/science/article/pii/S1385894713005469

[9] Vahabi, H.; Ferry, L.; Longuet, C.; Otazaghine, B.; Negrell-Guirao, C.; David, G.; Lopez-Cuesta, J.-M., (2009) Combination effect of polyhedral oligomeric silsesquioxane (POSS) and a phosphorus modified PMMA, flammability and thermal stability properties, Materials Chemistry and Physics 136 (2-3): 762-770, http://www.sciencedirect.com/science/article/pii/S0254058412007018

[10] Yang, B.H.; Li, M.; Wu, Y.; Wan, X.L., (2013) Thermal and Mechanical Reinforcement of Poly(methyl methacrylate) via Incorporation of Polyhedral Oligomeric Silsesquioxane, Polymers & Polymer Composites 21(1)**:** 37-42 , http://apps.webofknowledge.com/full_record.do?product=WOS&search_mode=GeneralSearch&qid=18&SID=4DxysFgJfycStAHwqzi&page=1&doc=1

[11] Wang, L.J.; Xie, X.L.; Su, S.P.; Feng, J.X.; Wilkie C. A., (2010) A comparison of the fire retardancy of poly(methyl methacrylate) using montmorillonite, layered double hydroxide and kaolinite, Polymer Degradation and Stability 95(4)**:** 572–578, http://www.sciencedirect.com/science/article/pii/S0141391009004248

[12] Kong, Q.H.; Hu, Y.;Yang, L.; Fan, W.C.; Chen, Z.Y., (2007) Synthesis and properties of poly(methyl methacrylate)/clay nanocomposites using natural montmorillonite and synthetic Fe-montmorillonite by emulsion polymerization, Polymer Composites 27(1)**:** 49–54, http://onlinelibrary.wiley.com/doi/10.1002/pc.20156/abstract;jsessionid=F19D94E30D1AC9974E9C730B0F61A794.d01t04

[13] Wang, L.J.; Su, S.P.; Chen,D.; Wilkie, C. A., (2009) Variation of anions in layered double hydroxides: Effects on dispersion and fire properties, Polymer Degradation and Stability 94(5): 770–781, http://www.sciencedirect.com/science/article/pii/S0141391009000457

[14] Liu, X. Q., Wang, D. Y., Wang, X. L., Chen, L. and Wang,Y. Z.,(2011) Synthesis of Organo-modified Alpha-zirconium Phosphate and Its Effect on the Flame Retardancy of IFR Poly (lactic acid) Systems, Polymer Degradation and Stability 296(5):771-777, http://www.sciencedirect.com/science/article/pii/S0141391011001042

[15] Lu,H.D., Wilkie, C. A., Ding, M. and Song, L.,(2011) Flammability Performance of Poly(vinyl alcohol) Nanocomposites with Zirconium Phosphate and Layered Silicates, Polymer Degradation and Stability 96(7):1219-1224, http://www.sciencedirect.com/science/article/pii/S014139101100156X

[16] Echchahed, B., Jeannot, F.,Malaman, B. and Gleitzer, C.,(1988) Preparation and Study of a Low-temperature Variety of Mixed-valence Iron Oxyphosphate Beta-$Fe_2(PO_4)O$ and of $NICR(PO_4)O$-a Case of Rapid Electron-transfer, Journal of Solid State Chemistry 74(1):47-59,http://www.sciencedirect.com/science/article/pii/0022459688903301

[17] Schmid-Beurmann, P.,(2000) Synthesis and Phase Characterization of a Solid Solution Series between Beta-Fe-2(PO4)O and Fe-4(PO4)(3)(OH)(3), Journal of Solid State Chemistry 153(2):237-247, http://www.sciencedirect.com/science/article/pii/S0022459600987474

[18] Nabi,S.A. And Siddiqui,Z.M.,(1985) Preparation, Properties, and Analytical Applications of Crystalline Tin(iv) Tungstoselenate, Bulletin of the Chemical Society of Japan 58(2):724-730, https://www.jstage.jst.go.jp/article/bcsj1926/58/2/58_2_724/_article

[19] Rawat,J.P. and Ansari, A.A.,(1990) Synthesis and Ion-exchange Properties os Sodium Stannosilicate-a

Silver Selective Inorganic-ion Exchanger, Bulletin of the Chemical Society of Japan 63(5):1521-1525, https://www.jstage.jst.go.jp/article/bcsj1926/63/5/63_5_1521/_article

[20] Bamford, C.H., Jenkins, A.D. and Johnston, R.,(1962) Initiation of Vinyl Polymerization and Interaction of Radicals with Ferric Chloride, Transactions of the Faraday Society 58(474):1212-1225,http://pubs.rsc.org/en/Content/ArticleLanding/1962/TF/tf9625801212

[21] Hatada, K., Kityama, T., Fujimoto, N. and Nishiura, T.,(1993) Stability and degradation of polymethacrylates with controlled structure, Journal of Macromolecular Science Pure and Applied Chemistry 30(9-10): 645-667, http://www.tandfonline.com/doi/abs/10.1080/10601329308021252#.UYTIOtCS2M8

[22] Schwan, J., Ulrich, S., Batori, V., Ehrhardt, H. and Silva, S.R.P.,(1996) Raman Spectroscopy on Amorphous Carbon Films, Journal of Applied Physics 180:440-447, http://jap.aip.org/resource/1/japiau/v80/i1/p440_s1

[23] Tamor, M.A. and Vassell; W.C.,(1994) Raman Fingerprinting of Amorphous-carbon Films, Journal of Applied Physics 76(6):3823-3830, http://jap.aip.org/resource/1/japiau/v76/i6/p3823_s1

[24] Tuinstra, F. and Koenig, J.L.,(1970) Raman Spectrum of Graphite, Journal of Chemical Physics 53(3):1126-1133,http://jap.aip.org/resource/1/japiau/v80/i1/p440_s1

[25] Kellogg, C.B. and Irikura, K.K.,(1999) Gas-Phase Thermochemistry of Iron Oxides and Hydroxides: Portrait of a Super-Efficient Flame Suppressant. Journal of Physical Chemistry 103(8):1150-1159, http://pubs.acs.org/doi/abs/10.1021/jp9842749